

JOINT COUPLING DESIGN OF UNDERACTUATED GRIPPERS

Aaron M. Dollar

Division of Engineering and Applied Sciences
Harvard University
Cambridge, MA 02138, USA
adollar@deas.harvard.edu

Robert D. Howe

Division of Engineering and Applied Sciences
Harvard University
Cambridge, MA 02138
howe@deas.harvard.edu

ABSTRACT

This paper examines the nature of joint coupling in underactuated grippers for environments where object properties and location may not be well known. A grasper consisting of a pair of two-link planar fingers with compliant revolute joints was simulated as it was actuated after contact with a target object. The joint coupling configuration of the gripper was varied in order to maximize successful grasp range and minimize contact forces for a wide range of target object size and position. A normal distribution of object position was assumed in order to model sensing uncertainty and weight the results accordingly. The results show that proximal-distal joint torque ratios of around 0.6 produced the best results for cases in which sensory information available for the task was poor, and ratios of around 1.0 produced the best results for cases in which sensory information available for the task was good.

INTRODUCTION

After years of experimenting with complex, fully-articulated anthropomorphic hands, researchers have begun to embrace the idea that much of the functionality of a hand can be retained by careful selection of joint coupling schemes, reducing the number of actuators and the overall complexity of the grasping mechanism. Many of these grippers are ‘underactuated’, having fewer actuators than degrees-of-freedom. These types of hand have also been referred to as ‘adaptive’ or ‘selfadaptable’. Other simplified hands have fixed-motion coupling between joints, reducing the overall degrees-of-freedom of the mechanism. These two classes of simplified grippers can be easier to control, much lighter, and less expensive than their fully-actuated counterparts.

The very nature of unstructured environments precludes full utilization of a complex, fully-actuated hand. In order to appropriately use the added degrees of actuation, an accurate model of the task environment is necessary. A gripper with a reduced number of actuators is not only simpler to use, it is more appropriate based on the quality of information available for the unstructured grasping task.

The joint coupling necessary to allow for underactuation is often accomplished through compliance in the manipulator structure. Compliance is perhaps the simplest way to allow for coupling between joints without enforcing the fixed-motion coupling relationship inherent with gear or linkage couplings. Compliant couplings are a simple way to allow a joint to passively deflect without causing a fixed-motion proportional change in the joints to which it is coupled.

Compliant underactuated grippers show particular promise for use in unstructured environments, where object properties are not known *a priori* and sensing is prone to error. Finger compliance allows the gripper to passively conform to a wide range of objects while minimizing contact forces. Passive compliance offers additional benefits, particularly in impacts, where control loop delays may lead to poor control of contact forces [1,2]. Compliance can also lower implementation costs by reducing the sensing and actuation required for the gripper.

In previous work, we examined the optimization of the preshape and joint stiffness of simple two-fingered grippers with passive springs in the joints. This study showed that for a particular set of joint stiffnesses and rest angles, the widest range of range of uncertainty in object size and location could be allowed for. Contact forces were also minimized at approximately the same gripper configuration. In addition to simulation studies, these results were confirmed with experimental tests using a reconfigurable gripper [3].

In this paper, we explore the role of the joint coupling scheme in grasping in unstructured environments, where poor sensing may mean that object size and location uncertainty can span a wide range. In particular, we examine the performance of a two-fingered compliant underactuated gripper as joint torque ratio and joint compliance are varied. Performance is compared on the basis of the maximum range of object size and location that can be successfully grasped and the magnitude of contact forces.

We begin with a survey of underactuated and fixed-motion coupled robotic hands, describing in depth the nature of the coupling schemes and/or compliance in each. We then describe the details of the gripper and grasping scenario that we are studying. Finally we provide the results of a simulation of the

TABLE I
UNDERACTUATED AND FIXED-MOTION COUPLED ROBOT HANDS

Hand	#fingers	Pitch joints per finger	Pitch actuators per finger	Coupling scheme		Coupling ratio	Source of compliance and/or adaptability
				(*indicates compliant coupling	(^indicates adaptive mechanism)		
100G [4]	2	2	1/2	prox:*	:dist	unknown	tendon routing, spring-loaded joints
Barrett [5]	3	2	1	prox:*	:dist	(3:4)	"TorqueSwitch" differential
Belgrade/USC [6]	4+1	3+0	1/2+1	(prox;med;dist)+(prox;dist)		(~9:8;7)	rocker arm coupling of fingers
DLR I and II [7,8]	4	3	2	med;dist		(1:1)	none
Domo [9]	3	3	1	prox;med:*	:dist	(1:1:passive)	unactuated compliant distal joint
Graspar [10]	3	3	1	prox:*	:med:*	(~5:4.2:2.9)	tendon differential mechanism
Hirose [11]	2	10	1/2	prox:(all)	:distal	(55:::28:::10:::1)	tendon routing
Laval 10-DOF [12]	3	3	1/3	prox:*	:med:*	unknown	adaptive linkage mechanism
NAIST [13]	3+1	3+3	2+2	(med;dist)+(med;dist)		(1;1.15)	none
Obrero [14]	3	2	1	prox:*	:dist	(4:3)	series elastic actuation
Robonaut [15]	2+2+1	3+3+2	2+1+2	(med;dist)+(prox;med;dist)+0		(1;1)+(1;1;1)+0	compliant connector, no adaptability
Rutgers [16]	4+1	3+3	2+2	med;dist		unknown	tendon routing
Salford [17]	4+1	3+3	2+3	(med;dist)+0		unknown	none
SDM [18]	2	2	1	(prox:*	:dist)	(4.5:1)	tendon routing, joints made of springs
Shadow [19]	4+1	3+2	2+2	(med;dist)+0		unknown	McKibbons, unknown adaptability
Southampton [20]	3	3	1	prox:*	:med:*	unknown	differential unit
SPRING [21]	2+1	3+2	1/3+1/3	(prox:*	:med:*	(2.9:1.6:1)	series elastic actuation
TBM [22]	4+1	3+2	1+1	(prox;med;dist)+(prox;dist)		(~2;1;1)+(~2;1)	none
UB III [23]	2+2+1	3+3+3	3+2+2	0+(med:*	:dist)+(med:*	:dist) (~6:7)	tendon routing, joints made of springs

grasping process for a wide range of target object size and position, identifying optimal joint coupling schemes for various levels of sensory information available for the grasping task.

SURVEY OF UNDERACTUATED HANDS

Table I provides an overview of some of the most well-known underactuated and fixed-motion coupled robotic hands. An ‘underactuated’ hand has fewer actuators than degrees-of-freedom, and therefore demonstrates adaptive behavior. In these hands, motion of the distal links can continue after contact on the coupled proximal links occurs, allowing the finger to passively adapt to the object shape. In a ‘fixed-motion coupled’ hand, each actuator controls a single degree-of-freedom, and the mechanism has no ‘adaptability’ (final column). In these hands, motion of one joint always results in a proportional motion of the joint(s) coupled to it. In the same way, if contact occurs on one joint fixing its position, all coupled joints are thereby fixed.

The '# fingers' column gives the number of fingers of each different type used in the hand, separated by '+'. Cases where two types are given indicate that some number of identical fingers and one thumb are used in the design. Cases where three types are given mean that two different finger designs are used in addition to a thumb. For example, the Robonaut hand [15] incorporates two “grasping” fingers, two “dexterous” fingers, and a thumb.

The second column indicates the number of ‘pitch’ joints per finger, leaving out ‘yaw’ and ‘roll’ joints, if any exist. Entries correspond to the data in the ‘# fingers’ column. For the Robonaut hand, the grasping and dexterous fingers and thumb have three pitch joints each.

The next column corresponds to the number of actuators per finger that control the pitch joints. Note that the degree of underactuation ranges from a single actuator for twenty joints (Hirose’s “Soft Gripper” [11]) to twelve actuators for fifteen joints (UB III hand [23]).

The coupling scheme is indicated in the next column. ‘Prox’ indicates the proximal joint (nearest to the base), ‘med’ is the medial joint (for three phalanx fingers), and ‘dist’ is the distal joint (farthest from the base). A ‘*:’ between two joints indicates that the coupling between the two joints is compliant, such as those hands with joints made of springs. A ‘:^’ between two joints indicates that the coupling between the two joints is based on a mechanism that allows for decoupling. The BarrettHand [5], for example, achieves this effect by means of a “TorqueSwitch” differential gear mechanism that actively decouples the two joints once contact has been made on the inner link and a preset torque limit has been reached. A ‘;’ between joints indicates that the coupling is fixed-motion, and therefore has no adaptability.

The next column indicates the coupling ratio (prox:med:dist) between the joints. For a finger with some method of adaptability, this ratio is the relative angular motion between joints when the finger is freely actuated (i.e. no external contact). For Hirose’s “Soft Gripper” [11], every third value is given.

The final column indicates the method by which the hand is passively compliant and/or adaptive, if at all.

METHODS

We select for this study a simple gripper with two fingers, each with two revolute degrees of freedom (Fig. 1). This gripper, proposed by Hirose [11], is perhaps the simplest

TABLE II
NOMENCLATURE

parameter	definition
ϕ_1, ϕ_2	spring rest link angles
ψ_1, ψ_2	deflected angles
$\Delta\psi_i$	small joint deflection due to fingerpad compliance
k_1, k_2	joint stiffness values
k_r	stiffness ratio (k_2/k_1)
k_s	finger skin stiffness
τ_1, τ_2	joint torque values
τ_r	torque ratio (τ_2/τ_1)
r	object radius
x_c	object position from the centerline
l	grasper link length
a_i	distance from joint i to contact point on link i
F_T	contact force tangential to the link surface
F_N	contact force normal to the link surface
F_{Ru}	unbalanced object force
μ	coefficient of friction
σ	standard deviation of object position

configuration that is able to grasp a wide range of objects. This mechanism is the same as that used in the 100G hand [4] and the SDM hand [18], and is similar to the planar, power-grasp configurations of the BarrettHand [5], Domo hand [9], Laval 10-DOF hand [12], Obrero hand [14], and SPRING hand [21], among others.

We use a planar analysis and assume that the links are rigid lines between joints and that each joint of the gripper includes a passive torsional spring providing a rotationally compliant joint. Our goal is to determine how variations in the joint coupling schemes affect the ability to grasp objects in the presence of uncertainty. For this purpose, we must define the scenario in which the grasper will operate.

Grasp Scenario

The basic grasping process follows a simple scenario. We assume that sensing (e.g. vision) provides rudimentary information about the target object location, and that the robot arm or vehicle moves straight towards this location. As the robot advances, the grasper comes into contact with an object with unknown properties and location. At this point the robot stops its forward progress and the joints of the gripper are actuated to bring both fingers into contact with the object, securing the grasp.

In order to simplify the analysis, we ignore inertial effects and assume quasi-static conditions. To simplify the geometrical calculations, the links were assumed to be simple lines through the joint axes. The object to be grasped was assumed to be circular (a frequent assumption in the grasping literature, and a reasonable approximation for many objects), and sufficiently massive such that the gripper contact forces do not displace or rotate it.

Detailed steps of the grasping scenario are as follows: the grasper has some joint angle preshape of $\phi_1, \phi_2, \phi_3, \phi_4$ (Fig 2, top). The robot moves forward, stopping when contact is made with a circular object of radius r at position x_c from the

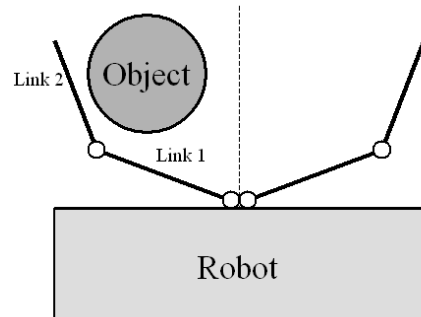


Fig. 1. A grasper mounted on a robot vehicle approaching an object to be grasped. The grasper consists of two fingers, each a 2 degree of freedom planar manipulator with revolute joints.

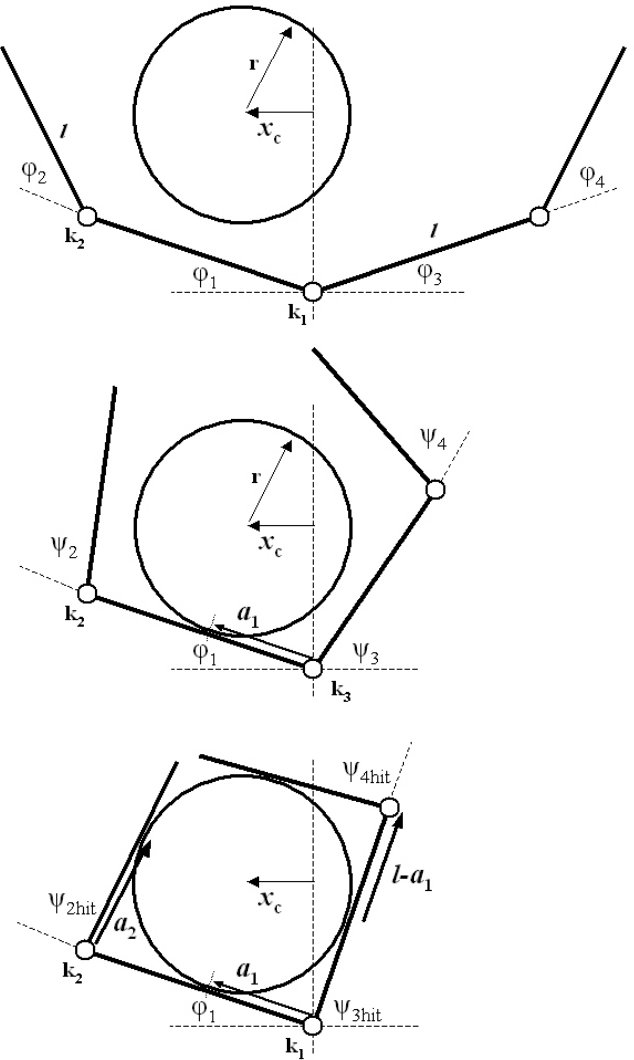


Fig. 2. Example grasping scenario with relevant terms

centerline of the grasper. Due to reasons explained in the results section, initial contact is always made on the proximal link. When contact has been made, the joints of the grasper are actuated to begin to enclose the object (Fig. 2 middle). Due to contact, the angle of the contact joint remains fixed

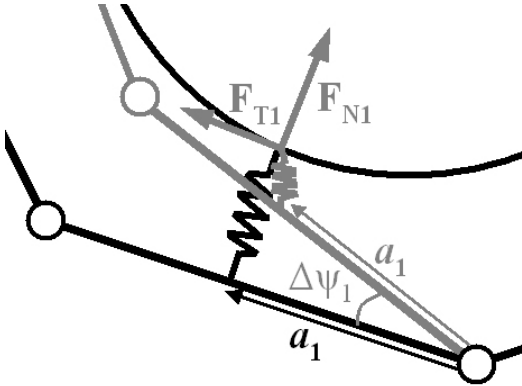


Fig. 3. Spring model of the elastic finger skin after undergoing a virtual displacement, with relevant terms.

$$\psi_1 = \varphi_1$$

where ψ is the deflected joint angle.

When actuated by a joint torque τ , the other joints move in proportion to their stiffness, k

$$\psi_i = \frac{\tau_i}{k_i} - \varphi_i, \quad i=2,3,4$$

until contact with the object on the respective link has been made (Fig 2 bottom). The joint angles at contact (ψ_{hit}) can be found

$$r \sin \psi_{3hit} - a_3 \cos \psi_{3hit} - x_c = 0$$

where a_3 is the lever arm length on link 3

$$a_3 = a_1 = \frac{x_c + r \sin \psi_1}{\cos \psi_1}.$$

When contact on the two inner links is made, the outer joints continue to close against the object until they have made contact

$$\psi_{2hit} = \psi_{4hit} = \pi - 2 \tan^{-1} \left(\frac{r}{l-a_1} \right)$$

This relationship comes from the symmetry of the two fingers when in complete contact with the object (Fig. 2 bottom) and that

$$a_2 = l - a_1.$$

The gripper is assumed to be covered with an elastic, high-friction skin to increase grasp stability [24,25]. This skin is modeled as a linear spring (with stiffness k_s) positioned along the normal to the link surface with some contact friction, μ . (Fig. 3) As torque (τ_j) is increased after contact has been made, small deflections ($\Delta\psi_j$) of the joint cause the spring to deflect and exert force on the object (F_{Nj} and F_{Tj})

$$F_{Nj} = (\tau_j - k_s(\psi_j - \varphi_j)) / a_j$$

$$\Delta\psi_j = \sin^{-1} \left(\frac{F_{Nj}}{a_j k_s} \right), \quad j = 1,3.$$

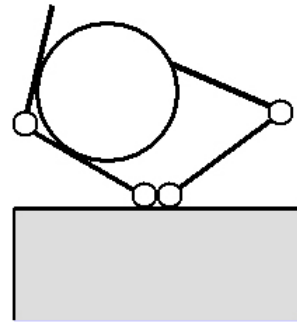


Fig. 4. Example of an unsuccessful grasp

These small joint deflections are assumed to be insignificant displacements of the joints and do not affect grasper kinematics. However, they are required to calculate contact forces.

The resulting tangential component of the object force is

$$F_{Tj} = a_j k_s (1 - \cos \Delta\psi_j), \quad j = 1,3$$

for $F_{Tj} \leq \mu_s F_{Nj}$. For cases when the coefficient of static friction has been overcome at the contact point, $F_{Tj} = \mu_s F_{Nj}$.

Total force on the object is defined as the sum of forces at the individual contact points. For the stages of the grasping process before the outer links have made contact, this force is nonzero and must be balanced by a ground reaction force for the object to remain in equilibrium. Nonzero object force will henceforth be referred to as unbalanced object force (F_{Ru}), and will be used as a quality measure that should be minimized.

The actuation considered in this study is analogous to the scheme considered by Hirose [11] and implemented by Kaneko [4]: a single actuator for the four joints (two joints on two fingers). In this type of configuration, both joints on the same finger are coupled in some ratio. Assuming the transmission configuration in the two fingers is the same,

$$\tau_1 = \tau_3 \text{ and } \tau_2 = \tau_4.$$

Parametric Analysis

The grasping scenario was simulated for a wide range of grasper parameter values, recording contact forces and the successful grasp range across a range of joint coupling configurations. The algorithm, implemented in Matlab (The Mathworks, Natick, MA), found the joint angles and object contact forces as joint torques were increased using the above system of equations. Simulation of the grasping process continued until both fingers enclosed the object.

The simulation was used to investigate the performance across the space of design parameters. The joint stiffnesses were applied as a ratio, since the individual magnitudes only affect the magnitude of the applied force and not the deflection behavior of the mechanism. In order to apply the actuation coupling that exists for this mechanism, individual joint torques were also applied as a ratio. Therefore, as the distal joint is being brought into contact with the object, the proximal joint applies force to the object due to non-zero torque about that joint. The ratios are defined as follows

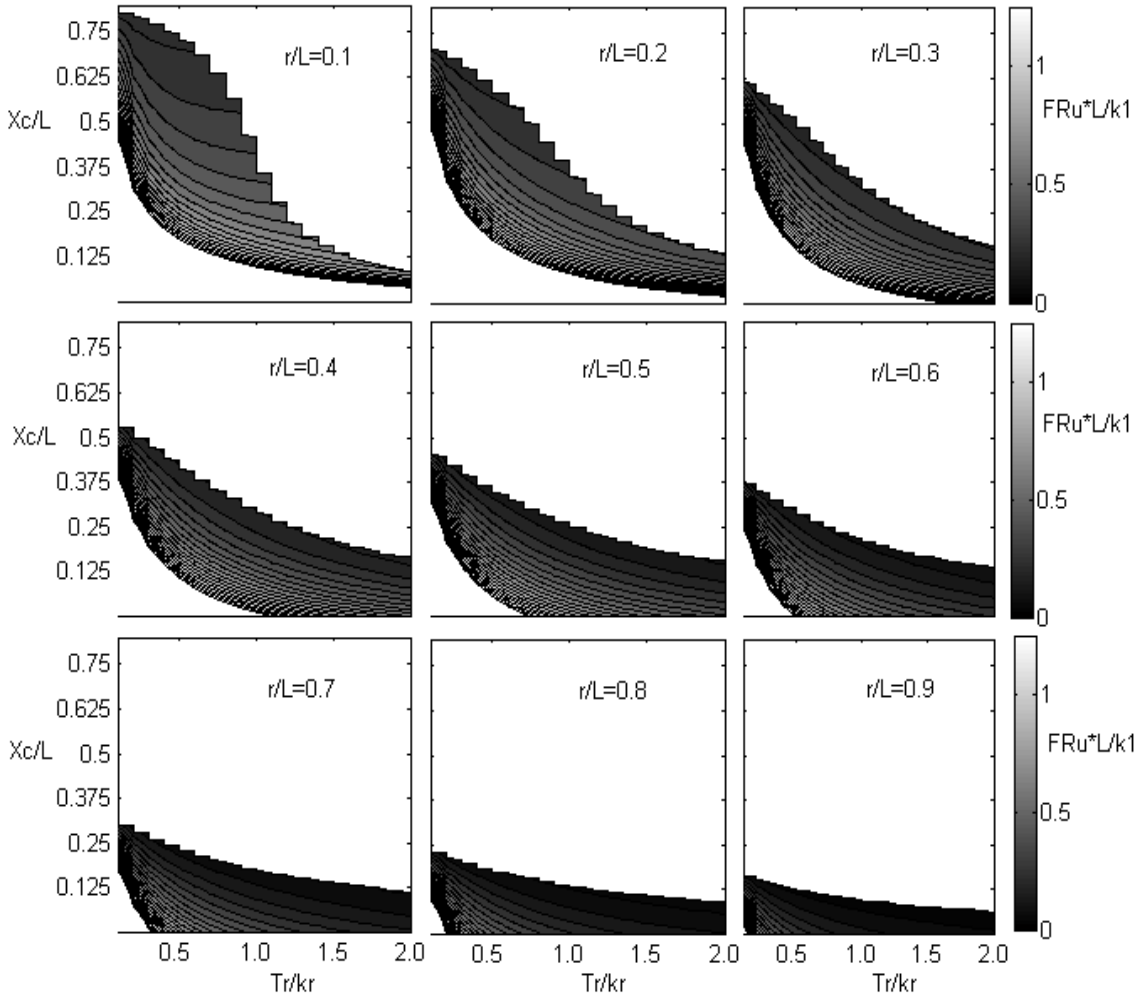


Fig. 5 Unbalanced object force (F_{Ru}) as object location (x_c/l) and size (r/l) are varied for a range of torque ratio values (τ_r/k_r).

$$\tau_r = \frac{\tau_2}{\tau_1} = \frac{\tau_4}{\tau_3} \text{ and } k_r = \frac{k_2}{k_1} = \frac{k_4}{k_3}.$$

The motion that results when a compliant gripper is actuated is a function of both the torque and the joint stiffness. Therefore, for the purposes of this study, the torque ratio will be normalized by the stiffness ratio for an independent variable (τ_r/k_r). From this point forward, this independent variable will be referred to simply as ‘torque ratio’. Note that for conditions in which object contact has not been made on the specified finger

$$\frac{\tau_r}{k_r} = \frac{\psi_2 - \varphi_2}{\psi_1 - \varphi_1},$$

representing the angular coupling under free actuation.

The object parameters x_c and r are varied to test the scenario of grasping an unfamiliar object at an unknown location. Distances were normalized by l , the link length. The performance of the gripper for each torque ratio configuration was evaluated for normalized object radius, $r/l = \{0.1:0.1:0.9\}$ and object location, x_c/l , incremented by 0.0025 from the center

toward the outside of the grasping range. The maximum normalized distance of the object from the centerline for which a successful enveloping grasp was attained (x_{cmax}) was recorded for each configuration. This value represents the successful grasp range.

The largest force applied to the object during the grasping process before complete object enclosure was also recorded for each tested value of object location, x_c/l . The overall goal is to determine the coupling scheme (torque ratio, τ_r/k_r) that results in the lowest unbalanced object forces and the largest grasp range.

It is assumed that the fingers will not interfere with each other when the links overlap, as is the case if they are slightly offset in the out-of-plane direction. The static and kinetic friction coefficients were set equal to further reduce the dimension of the parameter space. The coefficient of friction was tested at $\mu=2$, based on previous studies that suggest high friction increases grasp stability [24,25]. The default rest angle configuration was $\varphi_1, \varphi_2 = (25, 45)$ ° and was based on the results of a previous study [3]. We do, however, examine the behavior of the gripper mechanism for other gripper preshapes as described at the end of the ‘results’ section.

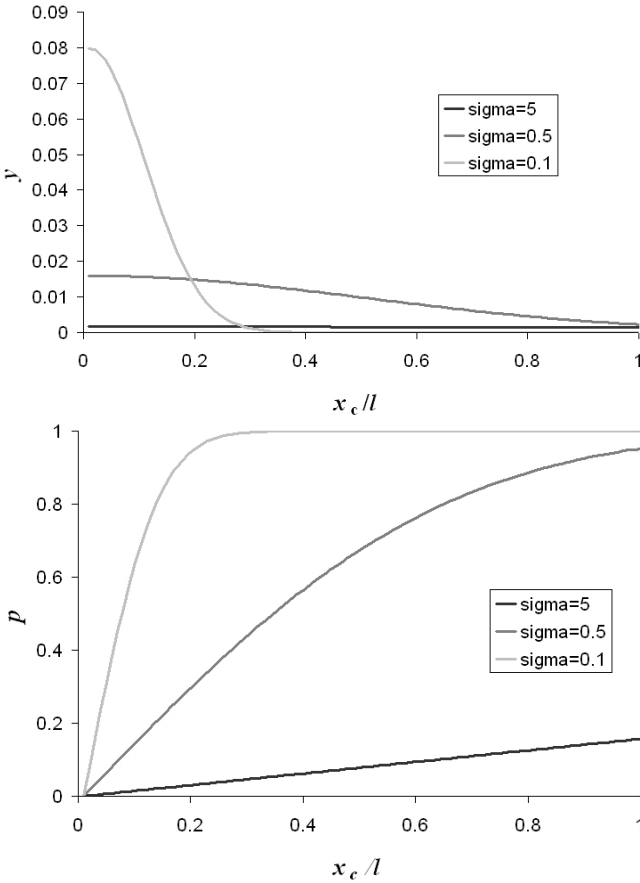


Fig. 6. Gaussian distribution and probability functions for x_c/l for three different values of standard deviation (mean=0).

Cases in which tip contact on one finger occurs are judged as unsuccessful grasps (Fig. 4). These cases typically occur at high torque ratios and most often result in the tip slipping and folding in towards the base joint after continued actuation, due to the large relative torque about joint 4.

RESULTS

Fig. 5 shows the results of the simulation for nine different object radius values. Maximum unbalanced object force (F_{Ru}) was recorded as object position (x_c/l) and torque ratio (τ_r/k_r) were varied. Note that the white portions in the upper right of each plot are unsuccessful configurations (no grasp could be achieved), whereas the white areas in the lower left are regions of large F_{Ru} .

These results suggest that, to keep unbalanced object forces low, torque ratio (τ_r/k_r) should be as large as possible. However, as torque ratios (τ_r/k_r) increase, the position range in which an object can be successfully grasped ($\max(x_c/l)$) is decreased. This range ($\max(x_c/l)$) is the outer boundary of the contour plots in fig. 5.

This tradeoff in force versus successful grasp range can be weighed by considering the quality of the sensory information available for the grasping task. For a task in which the location of the target object is well known, the torque ratio can be large, since the gripper can be reliably centered on the object. For this case, the gripper does not need to be able to grasp objects at positions far from the centerline.

However, for tasks in which sensory information is poor, the positioning of the gripper is subject to large errors, requiring that the chosen torque ratio should allow for positions far from the centerline (x_c/l).

Weighted Results

The results of Fig. 5 are further analyzed by weighting the individual data points by a normal distribution of the target object position, x_c/l , for a number of values of standard deviation. Different values of standard deviation of x_c/l correspond to different qualities of sensory information about the object prior to contact (e.g. vision) – large standard deviation corresponding to poor sensing and small standard deviation corresponding to good sensing.

Weighting functions were generated according to the normal, Gaussian distribution (for a mean of zero)

$$y(x) = \frac{1}{\sigma\sqrt{2\pi}} e^{\frac{-x^2}{2\sigma^2}}$$

with normal probability density of

$$p(x) = \int y(x) dx,$$

where $x = x_c/l$. Weighting functions for the three tested values of standard deviation ($\sigma = 5, 0.5, 0.1$) are shown in Fig. 6.

The normal distribution function was used to calculate a weighted average ($\bar{Q}_{F_{Ru}}$) of the maximum unbalanced object force over the range of object positions (x_c/l) for a given torque ratio (τ_r/k_r)

$$\bar{Q}_{F_{Ru}}(\tau_r/k_r) = \sum_i \tilde{F}_{Ru}(\tau_r/k_r, i)$$

$$\text{where } \tilde{F}_{Ru}(\tau_r/k_r, x_c/l) = \frac{F_{Ru}(\tau_r/k_r, x_c/l)y(x_c/l)}{\sum_i y(x_c/l)_i}$$

Fig. 7 shows the results of this weighting across a wide range of object size for two different standard deviations (top plots - $\sigma = 5, 0.1$), as well as an average over all tested object sizes ($r/l = 0.1, 0.2, \dots, 0.9$) for three different standard deviations ($\sigma = 5, 0.5, 0.1$). For all cases except $\sigma = 5$, $r/l = 0.1$, the minimum unbalanced object force is achieved by maximizing the torque ratio (τ_r/k_r).

To address the tradeoff that high torque ratio leads to low grasp range, the normal probability density function was used to calculate a quality measure of the successful grasp range ($Q_{X_{cmax}}$) for a given torque ratio (τ_r/k_r)

$$Q_{X_{cmax}}(\tau_r/k_r) = \left(\frac{x_{cmax}(\tau_r/k_r)p(x_{cmax}(\tau_r/k_r))}{\sum_i p(x_{cmax}(\tau_r/k_r))_i} \right)^{-1}$$

The inversion of the grasp space quality measure serves to allow for comparison between the unbalanced force quality measure – a lower value represents a more desirable configuration. Without the inversion, this term represented the

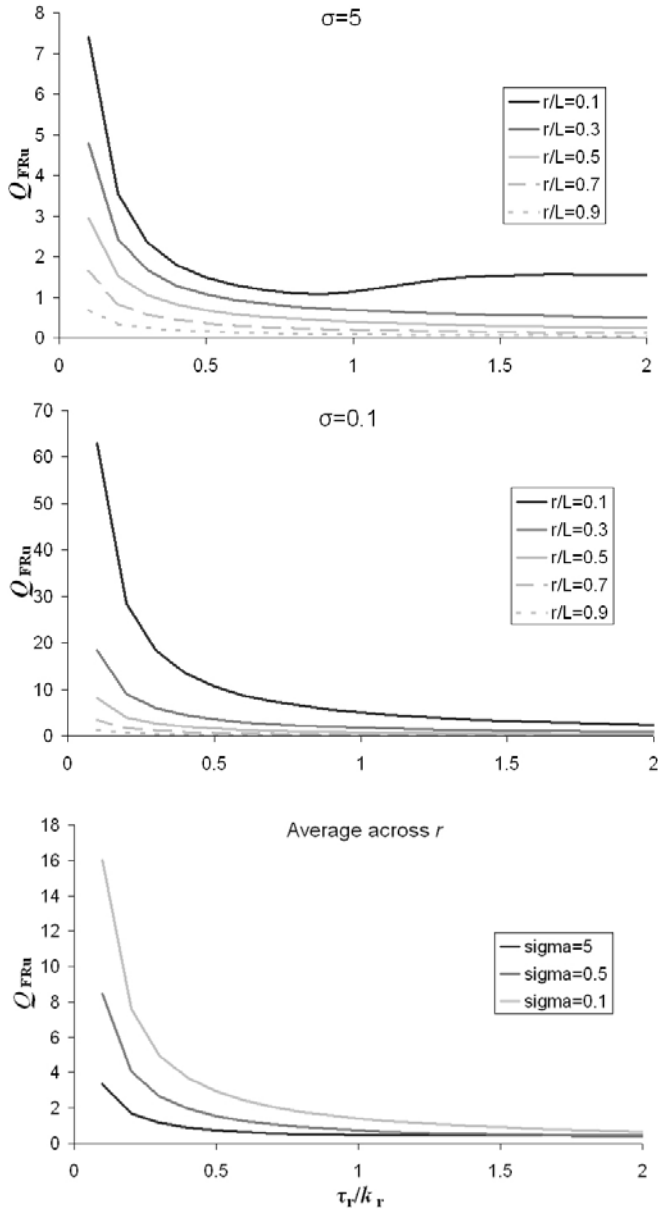


Fig. 7. Force quality for $\sigma=5$, $\sigma=0.1$, and averaged across object radius, r/l .

probability that a given torque ratio configuration will be able to successfully grasp an object with the specified position distribution.

It should be noted that the successful grasp range results show that a successful grasp can only be achieved for object positions in which initial contact is made with the inner (proximal) link. However, initial contact on the proximal link does not guarantee a successful grasp, as the successful grasp range for any coupling configuration is always less than the maximum position resulting in proximal link contact.

The top two plots in Fig. 8 show the results of grasp space quality across a wide range of object size for two different standard deviations ($\sigma = 5, 0.1$). Note that the “steps” in the $r/l=0.9$ curves are an artifact of the discrete incrementation of the values of object location and applied joint torque.

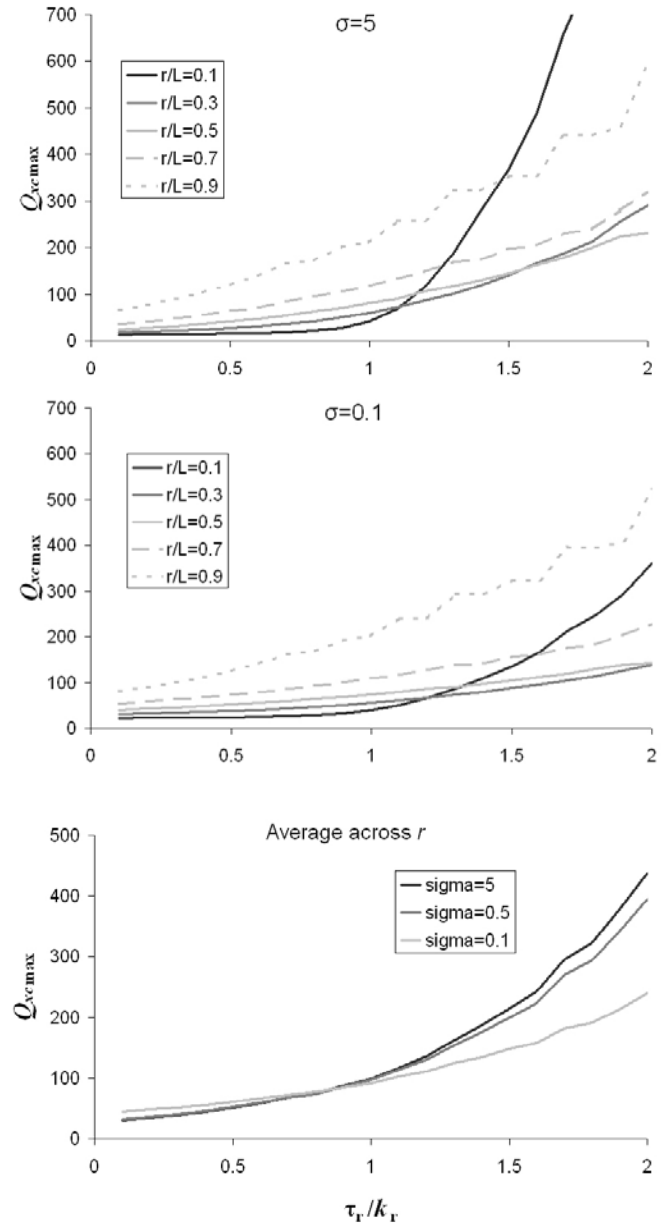


Fig. 8. Grasp range quality for $\sigma=5$, $\sigma=0.1$, and averaged across object radius, r/l .

The bottom plot is an average over all tested object sizes ($r/l=0.1, 0.2, \dots, 0.9$) for three different standard deviations ($\sigma=5, 0.5, 0.1$). These results show that by minimizing torque ratio, the maximum grasp space ($x_{c\max}$) can be achieved.

In order to provide a quantified sense of the tradeoffs between minimizing force and maximizing grasp space, the product of the two quality measures can be analyzed:

$$Q_{prod}(\tau_r/k_r) = \frac{\sum_i Q_{F_{Ru}}(\tau_r/k_r) Q_{x_{c\max}}(\tau_r/k_r)}{\sum_i Q_{x_{c\max}}(i)}$$

By calculating a total quality measure in this specific way, we are using the grasp space quality measure as a weighting function on the force quality. In this scheme, all weighting

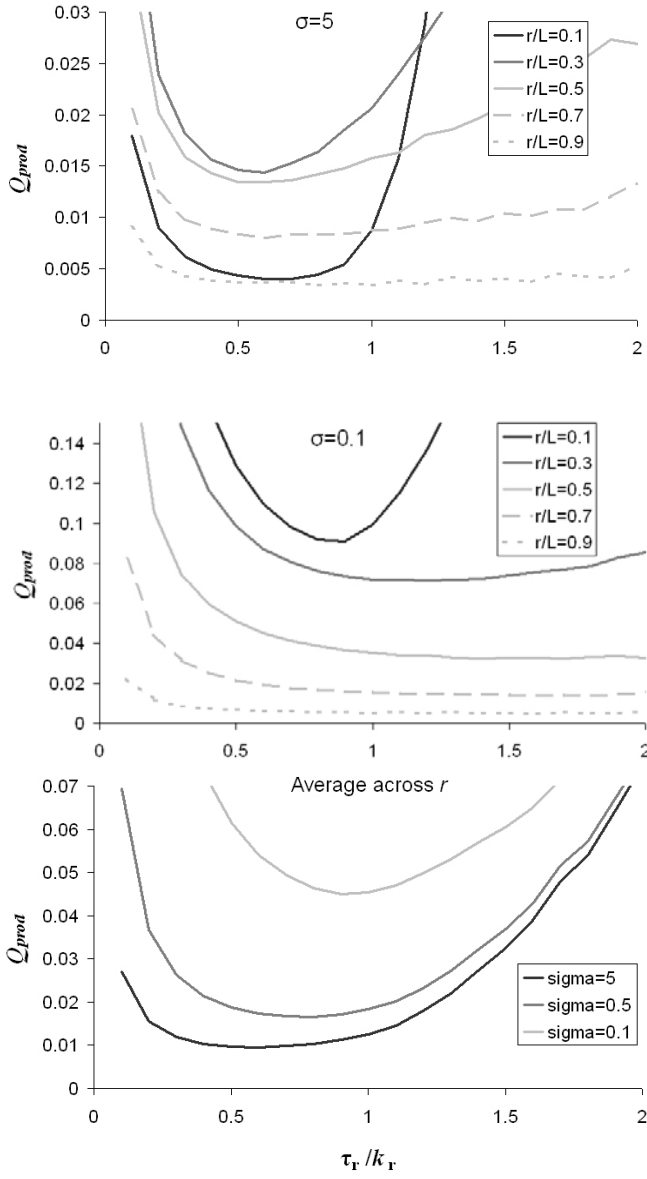
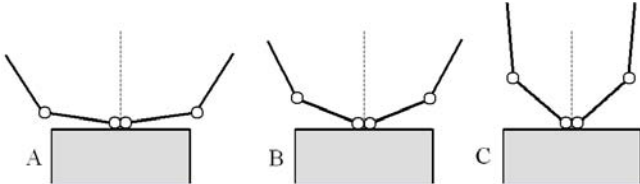


Fig. 9. Total quality for $\sigma=5$, $\sigma=0.1$, and averaged across object radius, r/l .



functions are based on the normal distribution of object position.

Fig. 9 shows Q_{prod} across a wide range of object size for two different standard deviations (top plots - $\sigma=5, 0.1$), as well as an average over all tested object sizes ($r/l=0.1, 0.2, \dots, 0.9$) for three different standard deviations ($\sigma=5, 0.5, 0.1$). For a large standard deviation in object position (poor sensing), there is a

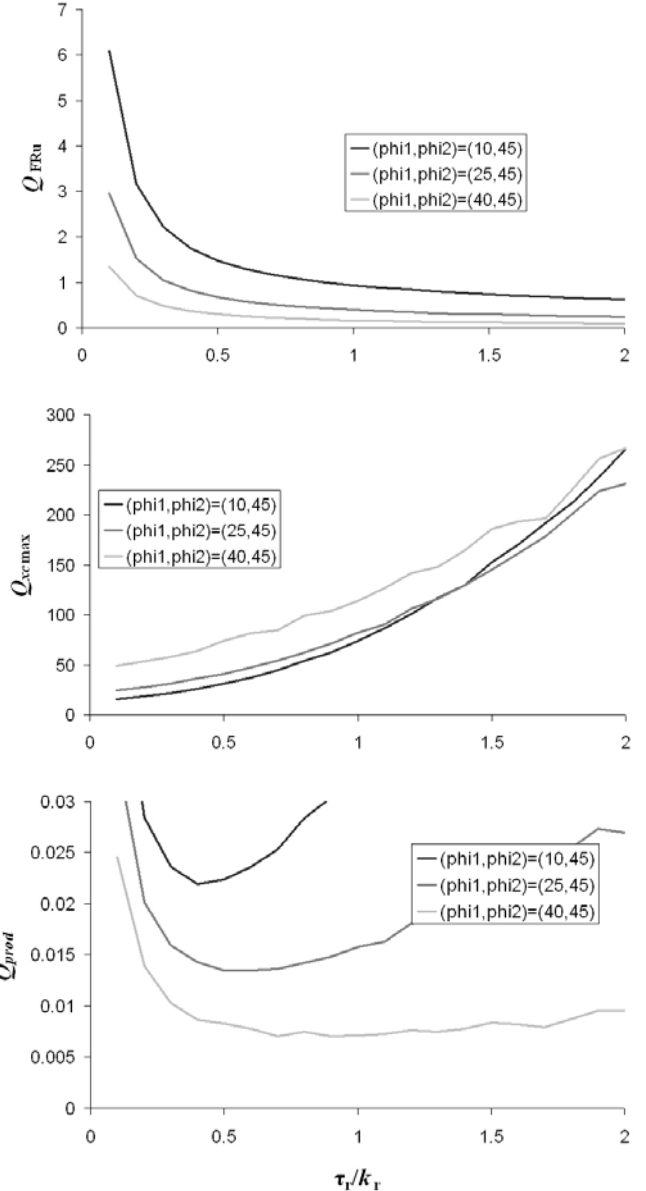


Fig. 11. Quality measures for variations in grasper preshape. $r/l=0.5$ and $\sigma=5$

clear optimum at around $(\tau_r/k_r) = 0.6$, and is consistently around this value across a wide range of object sizes. As the standard deviation is lowered (better sensing), this optimum shifts towards $\tau_r/k_r = 1.0$, and becomes more sensitive to object size. Indeed, for $\sigma=0.1$, there is no clear optimum for larger objects, although τ_r/k_r should be greater than 0.5.

In order to evaluate the sensitivity of these results to grasper preshape, we generate comparative results for variations about rest configuration, ϕ_1 and ϕ_2 . Fig. 10 shows the three configurations tested $\phi_1, \phi_2 = (10, 45^\circ), (25, 45^\circ), (40, 45^\circ)$. These configurations represent variations of ± 15 degrees of ϕ_1 from the default configuration 'B' $\phi_1, \phi_2 = (25, 45^\circ)$.

Fig. 11 shows the performance of the three different gripper preshapes for grasping an object of radius $r/l=0.5$ and standard deviation, $\sigma=5$. As ϕ_1 increases, average unbalanced object force decreases (Fig 11 top). At the same time, the grasp range of the gripper decreases, which is represented by an

increase in $Q_{X_{\max}}$ (Fig. 11 middle). From the product of the quality measures (Q_{prod}) it can be seen that as ϕ_1 increases, the optimum torque ratio shifts to a higher value.

CONCLUSIONS AND FUTURE WORK

We have described the evaluation of a simple, two-fingered underactuated gripper as it was actuated after contact with a target object. The joint coupling configuration of the gripper was varied in order to find the maximum successful grasp range while minimizing contact forces for a wide range of target object size and position. We showed that proximal-distal joint torque ratios of around 0.6 produced the best results for cases in which sensory information available for the task was poor, and ratios of around 1.0 produced the best results for cases in which sensory information available for the task was good.

This study was based on a specific grasping scenario, in order to limit the scope of the problem of grasping in an unstructured environment. While a complete understanding of the issues will require exploration of alternative scenarios, these results appear to hold for relaxation of some of the assumptions. For example, sensing has been treated here in a simplified fashion, with the assumption that once contact is made, sensors will detect this condition, the robot will be immediately stopped, and the gripper actuated. Preliminary results have shown that further forward travel of the robot for some distance after contact is achieved does not greatly affect the optimum grasper configuration and joint coupling.

Other issues that we will address include the expansion of the grasp scenario for the case in which a separate actuator is used for each finger. In this scenario, the unbalanced object force will be much smaller due to the fact that the finger on which initial contact occurs can remain unactuated until the second finger is brought into contact with the object. We would also like to include non-circular object shapes. However, preliminary consideration suggests that the optimum configurations found in this study apply to a range of convex objects.

ACKNOWLEDGMENT

This work was supported by the Office of Naval Research grant number N00014-98-1-0669.

REFERENCES

- [1] D. E. Whitney, "Quasi-static assembly of compliantly supported rigid parts," *Journal Dyn. Syst. Measurement Control* 104, pp. 65–77, 1982.
- [2] S. J. M. Schimmels and S. Huang, A passive mechanism that improves robotic positioning through compliance and constraint, *Robotics Comput.-Integr. Manuf.* 12 (1), 65–71, 1996.
- [3] A. M. Dollar and R. D. Howe, "Towards grasping in unstructured environments: Grasper compliance and configuration optimization," *Advanced Robotics, special issue on Compliant Motion*, vol. 19 (5), pp. 523-544, 2005.
- [4] M. Higashimori, M. Kaneko, A. Namiki, M. Ishikawa, "Design of the 100G Capturing Robot Based on Dynamic Preshaping," *The International Journal of Robotics Research*, vol. 24 (9), pp. 743-753, 2005.
- [5] W. T. Townsend, "The BarrettHand Grasper - Programmably Flexible Part Handling and Assembly," *Industrial Robot – An International Journal*, vol 10 (3), pp. 181-188, 2000.
- [6] M. Rakic, "Multifingered Robot Hand with Self-Adaptability," *Robotics and Computer Integrated Manufacturing*, vol. 5(2/3), pp. 269-276, 1989.
- [7] J. Butterfass, G. Hirzinger, S. Knoch, H. Liu, "DLR's Multisensory Articulated Hand Part I: Hard- and Software Architecture," *Proceedings of the 1998 IEEE International Conference on Robotics and Automation*, pp. 2081-2086, 1998.
- [8] J. Butterfass, M. Grebenstein, H. Liu, G. Hirzinger, "DLR-Hand II: Next Generation of a Dextrous Robot Hand," *Proceedings of the 2001 IEEE International Conference on Robotics and Automation*, pp. 109-114, 2001.
- [9] A. Edsinger-Gonzales, "Design of a Compliant and Force Sensing Hand for a Humanoid Robot," *Proceedings of the 2004 International Conference on Humanoid Manipulation and Grasping (IMG04)*, 2004.
- [10] J. Crisman, C. Kanjia, I. Zeid, "Graspar: A Flexible, Easily Controllable Robotic Hand," *IEEE Robotics and Automation Magazine*, pp. 32-38, June 1996.
- [11] S. Hirose and Y. Umetani, "The Development of Soft Gripper for the Versatile Robot Hand," *Mechanism and Machine Theory*, vol. 13, pp. 351-359, 1978.
- [12] T. Laliberte, L. Birglen, C. Gosselin, "Underactuation in Robotic Grasping Hands," *Machine Intelligence & Robotic Control*, vol. 4 (3) pp. 1-11, 2002.
- [13] J. Ueda, Y. Ishida, M. Kondo, T. Ogasawara, "Development of the NAIST-Hand with Vision-based Tactile Fingertip Sensor," *Proceedings of the 2005 IEEE International Conference on Robotics and Automation*, pp. 2343-2348, 2005.
- [14] E. Torres-Jara, "Obrero: A platform for sensitive manipulation," *Proceedings of the 2005 IEEE-RAS International Conference on Humanoid Robots*, pp. 327-332, 2005.
- [15] C. S. Lovchik, M. A. Diftler, "The Robonaut Hand: A Dexterous Robot Hand for Space," *Proceedings of the 1999 IEEE International Conference on Robotics and Automation*, pp. 907-912, 1999.
- [16] K. DeLaurentis, C. Mavroidis, "Mechanical design of a shape memory allow actuated prosthetic hand," *Technology and Health Care*, vol. 10, pp. 91-106, 2002.
- [17] D. Caldwell, N. Tsagarakis, "Soft" grasping using a dexterous hand," *Industrial Robot: An International Journal* vol. 27 (3), pp. 194-199, 2000.
- [18] A. M. Dollar and R. D. Howe, "A Robust Compliant Grasper via Shape Deposition Manufacturing," *ASME/IEEE Transactions on Mechatronics*, vol. 11(2), 2006.
- [19] The Shadow Dextrous Hand, <http://www.shadowrobot.com>
- [20] R. Crowder, V. Dubey, P. Chappell, D. Whatley, "A Multi-Fingered End Effector for Unstructured Environments," *Proceedings of the 1999 IEEE International Conference on Robotics and Automation*, pp. 3038-3043, 1999.
- [21] M. C. Carrozza, C. Suppo, F. Sebastiani, B. Massa, F. Vecchi, R. Lazzarini, M. R. Cutkosky, P. Dario, "The SPRING Hand: Development of a self-Adaptive Prosthesis for Restoring Natural Grasping," *Autonomous Robots 16*, pp. 125-141, 2004.
- [22] N. Dechev, W. Cleghorn, S. Naumann, "Multiple finger, passive adaptive grasp prosthetic hand," *Mechanism and Machine Theory* 36, pp. 1157-1173, 2001.
- [23] F. Lotti, P. Tiezzi, G. Vassura, L. Biagiotti, G. Palli, C. Melchiorri, "Development of UB Hand 3: Early Results," *Proceedings of the 2005 IEEE International Conference on Robotics and Automation*, pp. 4499 – 4504, 2005.
- [24] K. B. Shimoga, A. A. Goldenberg, "Soft materials for robotic fingers," *Proceedings of the 1992 IEEE International Conference on Robotics and Automation*, pp. 1300-1305, 1992.
- [25] M. R. Cutkosky, J. M. Jourdain, P. K. Wright, "Skin materials for robotic fingers," *Proceedings of the 1987 IEEE International Conference on Robotics and Automation*, pp. 1649-1654, 1987.